

Phase diagram and metastability of the Ising model on two coupled networks

Maíra Bolfe¹, Lucas Nicolao² and Fernando L. Metz^{1,3,4}

¹Departamento de Física, Universidade Federal de Santa Maria, 97105-900 Santa Maria, Brazil

²Departamento de Física, Universidade Federal de Santa Catarina, 88040-900 Florianópolis, SC, Brazil

³Instituto de Física, Universidade Federal do Rio Grande do Sul, Caixa Postal 15051, 91501-970 Porto Alegre, Brazil

⁴London Mathematical Laboratory, 14 Buckingham Street, London WC2N 6DF, United Kingdom

Abstract. We explore the cooperative behaviour and phase transitions of interacting networks by studying a simplified model consisting of Ising spins placed on the nodes of two coupled Erdős-Rényi random graphs. We derive analytical expressions for the free-energy of the system and the magnetization of each graph, from which the phase diagrams, the stability of the different states, and the nature of the transitions among them, are clearly characterized. We show that a metastable state appears discontinuously by varying the model parameters, yielding a region in the phase diagram where two solutions coexist. By performing Monte-Carlo simulations, we confirm the exactness of our main theoretical results and show that the typical time the system needs to escape from a metastable state grows exponentially fast as a function of the temperature, characterizing ergodicity breaking in the thermodynamic limit.

Keywords: Random graphs, complex networks, disordered systems

1. Introduction

Due to our increasing capability of collecting and manipulating large amounts of data, it has become common sense that many real-world systems are arranged in network structures [1]. Examples of problems defined on networks are abundant in physics, biology, and finance, ranging from the inference of ecological associations between microbial populations [2, 3] to the prediction of collapses in interbank networks [4].

The study of phase transitions and critical phenomena in networked systems constitutes an important research topic within the realm of complex networks [5]. Such phase transitions can be divided in two main classes: structural phase transitions, which refer to macroscopic changes in the architecture features of networks, and phase transitions emerging due to the cooperative behaviour of many entities interacting

through the links of the network. Examples of structural phase transitions are the percolation and condensation transitions [5], while synchronization [6, 7] and formation of consensus in social systems [8] are typical examples of cooperative phenomena.

Spin models of statistical physics are prototypical in the study of the collective or cooperative behaviour of many interacting entities [9]. Since in this case the individual elements have a relatively simple mode of operation, one can usually deal with the intricate pattern of interconnections defining the network structure in a more detailed way [10], allowing to obtain qualitative conclusions about the collective behaviour of the system and the critical properties characterizing eventual phase transitions. In particular, the Ising model [9], where each elementary unit is represented by a binary variable, has been used to characterize the formation of consensus in social systems [11], opinion dynamics and social spreading phenomena (see [8] and references therein). In this context, each Ising spin represents an agent that is confronted with a binary decision or choice [12], which is taken based on the choice of the majority in its local neighbourhood. The graph connecting different spins reflects the social network structure, while the temperature mimics the uncertainties of the agents or their idiosyncratic beliefs.

More recently, it has been realized that many real-world networks frequently do not operate in isolation, but depend on the structure and dynamics of other networks [13, 14]. This is the typical situation, for instance, in infrastructure networks, where the communication, electric power stations, and transportation networks are coupled together [15], in such a way that failure of nodes in one network can lead to recursively disruption or malfunction of nodes on other networks, leading to a cascading of failures [16, 17]. Social networks are also commonly organized in modular or community structures [18], where the network is composed by sparsely coupled communities or subgroups, with individuals densely connected inside each community. Networks of mobile phone users [19] and of scientific collaborators [20] are typical examples of social networks with a modular structure.

The natural initial step to study the emergence of cooperative behaviour on coupled networks is to consider models with Ising spins. The effect of coupling two networks on the possible macroscopic states of the system has been considered in several works [21, 22, 23, 24, 25, 26, 27]. By performing Monte-Carlo simulations [22, 26, 27] and mean-field approximations [21, 23], it has been shown that two possible solutions in terms of the magnetization of each network coexist: the networks might be aligned (equal magnetizations) or anti-aligned (magnetizations with opposite signs), depending on the model parameters. While the aligned state corresponds to the formation of consensus in a social system, the anti-aligned state represents the coexistence of contrary opinions between two groups, which ultimately describes a polarized society. Since models with Ising spins give qualitative insights on real social systems, it is important to assess the robustness of the anti-aligned solution with respect to changes in the model parameters, to characterize the free-energy of the anti-aligned state in comparison to other solutions, and to study how its presence influences the dynamics of the system. Apart from

Monte-Carlo simulations suggesting the presence of metastable configurations on the pathway of coupled networks to the equilibrium [26], not much is known about any of the aforementioned aspects. Phase diagrams illustrating the effect of the average connectivities on the macroscopic behaviour are also absent from previous works [21, 23]. These limitations stem from the naive mean-field approach employed in references [21, 23], which leads to a set of fixed-point equations for the magnetizations of each network, valid strictly in the regime of large connectivities.

The aim of the present work is to fill this gap and fully explore the macroscopic behaviour of two interacting networks in contact with a source of thermal noise. We consider a model composed of Ising spins placed on the nodes of two interacting Erdős-Rényi random graphs, with a ferromagnetic coupling between any pair of spins. The model is simple enough to allow for a full analytical treatment and the results should yield valuable insights on the general behaviour of the Ising model on coupled networks. In other words, we expect our work serves as a benchmark for studying more sophisticated models.

By using the replica approach of disordered systems, we derive the exact expressions for the magnetizations of each network and for the free-energy of the system, which allows us to obtain complete phase diagrams that unveil the role of the topology on the coexistence between ferromagnetic and anti-aligned states in this model. In particular, the region where both solutions coexist is strongly suppressed by an increase of the number of links among the two networks (see figure 1). We also show that the model displays a zero-temperature paramagnetic phase, essentially due to the low average connectivity within each network and between them. From the calculation of the free-energy of the system, we show that the anti-aligned solution is always metastable and it appears discontinuously as the model parameters are varied, clarifying the stability properties of the macroscopic states in the coexistence region [21, 23]. By means of Monte-Carlo simulations, we study the role of the metastability on the relaxation of the model to the equilibrium state by calculating the average time τ the system needs to escape from a metastable initial state. The results for $\tau(T)$ as a function of the temperature T are described by the Vogel-Fulcher law $\ln \tau(T) \sim (T - T_0)^{-1}$, where the temperature T_0 consistently converges, for increasing system size, to the instability temperature below which metastable states are present in the thermodynamic limit. In the context of formation of consensus in social systems, our results indicate that, under certain conditions, two social groups can coexist with opposite opinions for remarkably long times, even if all interactions favour their agreement. The exactness of our theoretical findings is supported by Monte-Carlo simulations.

In the next section we define the model of coupled random graphs in equilibrium with a thermal bath. In section 3 we present the main steps of the replica approach and the final analytical expressions for the magnetizations of each network and the free-energy of the system. The phase diagram and the stability of the macroscopic states are considered in section 4, while the results obtained through Monte-Carlo simulations are discussed in section 5. We present some final remarks and perspectives in the last

section.

2. Random graph model of two coupled networks

The model is composed of $2N$ interacting Ising spins or state variables. The spins $\sigma_i = \pm 1$ ($i = 1, \dots, N$) and $\tau_i = \pm 1$ ($i = 1, \dots, N$) are coupled according to the following Hamiltonian

$$\mathcal{H}(\boldsymbol{\sigma}, \boldsymbol{\tau}) = -J_\sigma \sum_{i < j}^N c_{ij}^\sigma \sigma_i \sigma_j - J_\tau \sum_{i < j}^N c_{ij}^\tau \tau_i \tau_j - U \sum_{i < j}^N c_{ij}^I (\tau_i \sigma_j + \tau_j \sigma_i), \quad (1)$$

where $\boldsymbol{\sigma} = (\sigma_1, \dots, \sigma_N)$ and $\boldsymbol{\tau} = (\tau_1, \dots, \tau_N)$. The sum $\sum_{i < j}^N (\dots)$ runs over all distinct pairs of spins and the coupling strengths (J_σ, J_τ, U) are ferromagnetic.

The random variables c_{ij}^σ , c_{ij}^τ and c_{ij}^I determine the topology of the model. We set $c_{ij}^\sigma = 1$ ($c_{ij}^\tau = 1$) if there is an edge between spins σ_i (τ_i) and σ_j (τ_j), and zero otherwise. The same definition applies to c_{ij}^I , which is responsible for the topology of connections among the two networks: we have $c_{ij}^I = 1$ if there is an edge between τ_i and σ_j and between τ_j and σ_i , and $c_{ij}^I = 0$ otherwise. We consider the simplest network model, where these random variables are independently drawn from the distributions

$$P_\sigma(c_{ij}^\sigma) = \prod_{i < j} \left[\frac{c_\sigma}{N} \delta(c_{ij}^\sigma, 0) + \left(1 - \frac{c_\sigma}{N}\right) \delta(c_{ij}^\sigma, 1) \right], \quad (2)$$

$$P_\tau(c_{ij}^\tau) = \prod_{i < j} \left[\frac{c_\tau}{N} \delta(c_{ij}^\tau, 0) + \left(1 - \frac{c_\tau}{N}\right) \delta(c_{ij}^\tau, 1) \right], \quad (3)$$

$$P_I(c_{ij}^I) = \prod_{i < j} \left[\frac{c_I}{N} \delta(c_{ij}^I, 0) + \left(1 - \frac{c_I}{N}\right) \delta(c_{ij}^I, 1) \right], \quad (4)$$

with δ representing the Kronecker delta. Essentially, the model is composed of two interacting Erdős-Rényi random graphs [28], where a given spin interacts with a random subset of spins within its own graph and with a random subset of spins belonging to the second graph. The parameter $c_\sigma > 0$ ($c_\tau > 0$) is the average number of neighbours per node that belong to graph- σ (τ), while c_I controls the average number of edges per node connecting both graphs. In the limit $N \rightarrow \infty$, the number of edges per node within each network, namely $k_i^{(\sigma)} = \sum_{j=1(\neq i)}^N c_{ij}^\sigma$ and $k_i^{(\tau)} = \sum_{j=1(\neq i)}^N c_{ij}^\tau$, follows a Poisson distribution

$$p_\sigma(k) = \frac{c_\sigma^k \exp(-c_\sigma)}{k!}, \quad p_\tau(k) = \frac{c_\tau^k \exp(-c_\tau)}{k!}. \quad (5)$$

The number of edges $k_i^{(I)} = \sum_{j=1(\neq i)}^N c_{ij}^I$ connecting a node i in a certain network to the nodes of the other network also follows a Poisson distribution

$$p_I(k) = \frac{c_I^k \exp(-c_I)}{k!}. \quad (6)$$

The partition function of the system in equilibrium at temperature T reads

$$\mathcal{Z} = \sum_{\boldsymbol{\sigma}, \boldsymbol{\tau}} e^{-\beta \mathcal{H}(\boldsymbol{\sigma}, \boldsymbol{\tau})}, \quad (7)$$

with $\beta = T^{-1}$. Our main objective consists in calculating the free-energy per spin in the thermodynamic limit $N \rightarrow \infty$. Besides giving access to macroscopic observables, such as the magnetization of each random graph, the free-energy allows us to clearly identify the presence of metastable states. Assuming that, in the limit $N \rightarrow \infty$, the free-energy per spin f is a self-averaging quantity with respect to fluctuations in the random graph structure, we have that

$$f = - \lim_{N \rightarrow \infty} \frac{1}{2\beta N} \langle \ln \mathcal{Z} \rangle, \quad (8)$$

in which $\langle \dots \rangle$ denotes the average over the ensemble of random graphs, defined through eqs. (2-4).

3. The free-energy and the equations for the order-parameters

In order to calculate the ensemble average in eq. (8), we employ the replica method [29]

$$\langle \ln \mathcal{Z} \rangle = \lim_{n \rightarrow 0} \frac{1}{n} \ln \langle \mathcal{Z}^n \rangle. \quad (9)$$

Initially, n is considered to be an integer and positive exponent. After the ensemble average in eq. (9) has been evaluated and the limit $N \rightarrow \infty$ has been taken, the analytical continuation $n \rightarrow 0$ yields the free-energy per spin. This is the standard strategy pursued in the replica approach [29]. Since the microscopic states in this model are not frustrated, replica symmetry yields exact results for the macroscopic behaviour of the system. We remark that the cavity method [32, 33], also known as belief propagation in information theory [34], provides an alternative tool to derive the same exact results as obtained in this section (see eqs. (27), (28) and (29)).

The calculation of the replicated partition function $\langle \mathcal{Z}^n \rangle$ in the thermodynamic limit is analogous to previous models defined on random graphs [30, 31, 10], so that we just present here the main steps of the derivation. By computing the average over the random graph ensemble in eq. (9) and then introducing the order-parameters

$$P_1(\boldsymbol{\sigma}) = \frac{1}{N} \sum_{i=1}^N \delta_{\boldsymbol{\sigma}, \boldsymbol{\sigma}_i}, \quad \boldsymbol{\sigma} = (\sigma_1, \dots, \sigma_n), \quad (10)$$

$$P_2(\boldsymbol{\tau}) = \frac{1}{N} \sum_{i=1}^N \delta_{\boldsymbol{\tau}, \boldsymbol{\tau}_i}, \quad \boldsymbol{\tau} = (\tau_1, \dots, \tau_n), \quad (11)$$

$$P_{12}(\boldsymbol{\sigma}, \boldsymbol{\tau}) = \frac{1}{N} \sum_{i=1}^N \delta_{\boldsymbol{\tau}, \boldsymbol{\tau}_i} \delta_{\boldsymbol{\sigma}, \boldsymbol{\sigma}_i}, \quad (12)$$

we are able to decouple sites in the expression for $\langle \mathcal{Z}^n \rangle$, which can be recast in the integral form

$$\langle \mathcal{Z}^n \rangle \sim \int \mathcal{D}\{P, \hat{P}\} \exp \left(Ng \left[\{P, \hat{P}\} \right] \right), \quad (13)$$

with the integration measure

$$\mathcal{D}\{P, \hat{P}\} \equiv \prod_{\boldsymbol{\sigma}, \boldsymbol{\tau}} dP_1(\boldsymbol{\sigma}) dP_2(\boldsymbol{\tau}) dP_{12}(\boldsymbol{\sigma}, \boldsymbol{\tau}) d\hat{P}_1(\boldsymbol{\sigma}) d\hat{P}_2(\boldsymbol{\tau}) d\hat{P}_{12}(\boldsymbol{\sigma}, \boldsymbol{\tau}). \quad (14)$$

The functional $g[\{P, \hat{P}\}]$ reads

$$\begin{aligned}
g[\{P, \hat{P}\}] = & -\frac{1}{2}(c_\sigma + c_\tau + c_I) + i \sum_{\boldsymbol{\sigma}} P_1(\boldsymbol{\sigma}) \hat{P}_1(\boldsymbol{\sigma}) + i \sum_{\boldsymbol{\tau}} P_2(\boldsymbol{\tau}) \hat{P}_2(\boldsymbol{\tau}) + i \sum_{\boldsymbol{\sigma}\boldsymbol{\tau}} P_{12}(\boldsymbol{\sigma}, \boldsymbol{\tau}) \hat{P}_{12}(\boldsymbol{\sigma}, \boldsymbol{\tau}) \\
& + \frac{c_\sigma}{2} \sum_{\boldsymbol{\sigma}\boldsymbol{\sigma}'} P_1(\boldsymbol{\sigma}) P_1(\boldsymbol{\sigma}') \exp(\beta J_\sigma \boldsymbol{\sigma} \cdot \boldsymbol{\sigma}') + \frac{c_\tau}{2} \sum_{\boldsymbol{\tau}\boldsymbol{\tau}'} P_2(\boldsymbol{\tau}) P_2(\boldsymbol{\tau}') \exp(\beta J_\tau \boldsymbol{\tau} \cdot \boldsymbol{\tau}') \\
& + \frac{c_I}{2} \sum_{\boldsymbol{\sigma}\boldsymbol{\sigma}'} \sum_{\boldsymbol{\tau}\boldsymbol{\tau}'} P_{12}(\boldsymbol{\sigma}, \boldsymbol{\tau}) P_{12}(\boldsymbol{\sigma}', \boldsymbol{\tau}') \exp[\beta U(\boldsymbol{\sigma} \cdot \boldsymbol{\tau}' + \boldsymbol{\sigma}' \cdot \boldsymbol{\tau})] \\
& + \ln \left[\sum_{\boldsymbol{\sigma}\boldsymbol{\tau}} e^{-i\hat{P}_1(\boldsymbol{\sigma}) - i\hat{P}_2(\boldsymbol{\tau}) - i\hat{P}_{12}(\boldsymbol{\sigma}, \boldsymbol{\tau})} \right], \tag{15}
\end{aligned}$$

where the conjugate parameters \hat{P}_1 , \hat{P}_2 and \hat{P}_{12} have arisen from the integral representations of the Dirac delta functionals, used to introduce the order-parameters in the expression for $\langle \mathcal{Z}^n \rangle$. From now on, the n -dimensional vector $\boldsymbol{\sigma}$ ($\boldsymbol{\tau}$) encodes the states of a single spin σ_i (τ_i) in the n different replicas, as explicitly emphasized in eqs. (10) and (11). Unimportant factors, which give a vanishing contribution to the free-energy per spin in the limit $N \rightarrow \infty$, have been neglected in eq. (13).

The function $\langle \mathcal{Z}^n \rangle$ can now be evaluated through the saddle-point method. In the limit $N \rightarrow \infty$, the integral in eq. (13) is dominated by the values of $\{P, \hat{P}\}$ that extremize the functional $g[\{P, \hat{P}\}]$. Substituting eq. (9) in eq. (8) and performing the limit $N \rightarrow \infty$ through the saddle-point method, we obtain a formal expression for the free-energy per spin

$$2\beta f = -\lim_{n \rightarrow 0} \frac{1}{n} g[\{P, \hat{P}\}], \tag{16}$$

where $\{P, \hat{P}\}$ refers, from now on, to the specific values that extremize $g[\{P, \hat{P}\}]$. The saddle-point equations that determine $\{P, \hat{P}\}$ are derived by taking functional derivatives of $g[\{P, \hat{P}\}]$ with respect to $\{P, \hat{P}\}$

$$P_1(\boldsymbol{\sigma}) = \frac{1}{\mathcal{N}} \sum_{\boldsymbol{\tau}} \exp[-i\hat{P}_1(\boldsymbol{\sigma}) - i\hat{P}_2(\boldsymbol{\tau}) - i\hat{P}_{12}(\boldsymbol{\sigma}, \boldsymbol{\tau})], \tag{17}$$

$$P_2(\boldsymbol{\tau}) = \frac{1}{\mathcal{N}} \sum_{\boldsymbol{\sigma}} \exp[-i\hat{P}_1(\boldsymbol{\sigma}) - i\hat{P}_2(\boldsymbol{\tau}) - i\hat{P}_{12}(\boldsymbol{\sigma}, \boldsymbol{\tau})], \tag{18}$$

$$P_{12}(\boldsymbol{\sigma}, \boldsymbol{\tau}) = \frac{1}{\mathcal{N}} \exp[-i\hat{P}_1(\boldsymbol{\sigma}) - i\hat{P}_2(\boldsymbol{\tau}) - i\hat{P}_{12}(\boldsymbol{\sigma}, \boldsymbol{\tau})], \tag{19}$$

where \mathcal{N} is the normalization factor

$$\mathcal{N} = \sum_{\boldsymbol{\sigma}\boldsymbol{\tau}} \exp[-i\hat{P}_1(\boldsymbol{\sigma}) - i\hat{P}_2(\boldsymbol{\tau}) - i\hat{P}_{12}(\boldsymbol{\sigma}, \boldsymbol{\tau})]. \tag{20}$$

The conjugate parameters are given by

$$\hat{P}_1(\boldsymbol{\sigma}) = ic_\sigma \sum_{\boldsymbol{\sigma}'} P_1(\boldsymbol{\sigma}') \exp(\beta J_\sigma \boldsymbol{\sigma}' \cdot \boldsymbol{\sigma}), \tag{21}$$

$$\hat{P}_2(\boldsymbol{\tau}) = ic_\tau \sum_{\boldsymbol{\tau}'} P_2(\boldsymbol{\tau}') \exp(\beta J_\tau \boldsymbol{\tau}' \cdot \boldsymbol{\tau}), \tag{22}$$

$$\hat{P}_{12}(\boldsymbol{\sigma}, \boldsymbol{\tau}) = ic_I \sum_{\boldsymbol{\sigma}'\boldsymbol{\tau}'} P_{12}(\boldsymbol{\sigma}', \boldsymbol{\tau}') \exp[\beta U(\boldsymbol{\sigma} \cdot \boldsymbol{\tau}' + \boldsymbol{\sigma}' \cdot \boldsymbol{\tau})]. \tag{23}$$

From eqs. (16-23), we see that the free-energy per spin is fully determined by the self-consistent equations (17-19) for the order-parameters.

In order to compute the limit $n \rightarrow 0$ in eq. (16), one has to explicitly perform the sums over the replica Ising spins and unveil how $g[\{P, \hat{P}\}]$ depends on n , which is only possible if we make an assumption for the structure of the order-parameters. By considering there is one single thermodynamic state, each order-parameter is invariant with respect to permutations of the replica indexes [31] and all information about the fluctuations of the local magnetizations lies in the distribution of effective fields $h_i = \beta^{-1} \arctan(\langle S_i \rangle)$, where $\langle S_i \rangle$ denotes the average of a generic spin S_i with respect to thermal and random graph fluctuations. The simplest form that fulfills replica symmetry is a function of the magnetizations only, namely [31, 10]

$$P_1(\boldsymbol{\sigma}) = \int dh W_\sigma(h) \frac{\exp(\beta h \sum_{\alpha=1}^n \sigma_\alpha)}{[2 \cosh(\beta h)]^n}, \quad (24)$$

$$P_2(\boldsymbol{\tau}) = \int dh W_\tau(h) \frac{\exp(\beta h \sum_{\alpha=1}^n \tau_\alpha)}{[2 \cosh(\beta h)]^n}, \quad (25)$$

$$P_{12}(\boldsymbol{\sigma}, \boldsymbol{\tau}) = \int dudv W_{\sigma\tau}(u, v) \frac{\exp(\beta u \sum_{\alpha=1}^n \sigma_\alpha + \beta v \sum_{\alpha=1}^n \tau_\alpha)}{[4 \cosh(\beta u) \cosh(\beta v)]^n}. \quad (26)$$

The quantity $W_\sigma(h)$ ($W_\tau(h)$) is the distribution of effective fields on network- $\boldsymbol{\sigma}$ ($\boldsymbol{\tau}$), independently of the configuration of effective fields in network- $\boldsymbol{\tau}$ ($\boldsymbol{\sigma}$). The distributions $W_\sigma(h)$ and $W_\tau(h)$ are normalized, consistently with eqs. (10) and (11). The function $W_{\sigma\tau}(u, v)$ is the joint distribution of effective fields in both networks, where the argument u (v) refers to the possible outcomes for the effective fields in network- $\boldsymbol{\sigma}$ ($\boldsymbol{\tau}$). Besides the normalization of $W_{\sigma\tau}(u, v)$, we have to supplement eq. (26) with the conditions $\int du W_{\sigma\tau}(u, v) = W_\tau(v)$ and $\int dv W_{\sigma\tau}(u, v) = W_\sigma(u)$, which ensure the marginalization of $P_{\sigma\tau}(\boldsymbol{\sigma}, \boldsymbol{\tau})$ with respect to the spins of a given network, consistently with eqs. (10-12).

By substituting eqs. (24-26) in eq. (16), computing the trace over the Ising spins, and performing the limit $n \rightarrow 0$, we obtain the free-energy per spin

$$\begin{aligned} f &= c_\sigma \int dh dh' W_\sigma(h) W_\sigma(h') \mathcal{U}_\beta(h, h' | J_\sigma) + c_\tau \int dh dh' W_\tau(h) W_\tau(h') \mathcal{U}_\beta(h, h' | J_\tau) \\ &+ 2c_I \int dh dh' W_\tau(h) W_\sigma(h') \mathcal{U}_\beta(h, h' | U) - \frac{1}{2\beta} \sum_{k_\sigma, k_I=0}^{\infty} p_\sigma(k_\sigma) p_I(k_I) \\ &\times \int \left(\prod_{n=1}^{k_\sigma} du_n W_\sigma(u_n) \right) \left(\prod_{m=1}^{k_I} dv_m W_\tau(v_m) \right) \ln \left[\sum_{\gamma=\pm 1} \mathcal{G}_\gamma(u_1, \dots, u_{k_\sigma} | J_\sigma) \mathcal{G}_\gamma(v_1, \dots, v_{k_I} | U) \right] \\ &- \frac{1}{2\beta} \sum_{k_\tau, k_I=0}^{\infty} p_\tau(k_\tau) p_I(k_I) \int \left(\prod_{n=1}^{k_\tau} du_n W_\tau(u_n) \right) \left(\prod_{m=1}^{k_I} dv_m W_\sigma(v_m) \right) \\ &\times \ln \left[\sum_{\gamma=\pm 1} \mathcal{G}_\gamma(u_1, \dots, u_{k_\tau} | J_\tau) \mathcal{G}_\gamma(v_1, \dots, v_{k_I} | U) \right], \end{aligned} \quad (27)$$

where

$$\mathcal{U}_\beta(u, v | J) = \frac{1}{4\beta} \ln \left[\frac{1 + \tanh(\beta u) \tanh(\beta v) \tanh(\beta J)}{\cosh(\beta J)} \right],$$

$$\mathcal{G}_\gamma(u_1, \dots, u_K | J) = \prod_{n=1}^K \left[1 + \gamma \tanh(\beta u_n) \tanh(\beta J) \right],$$

with $\gamma \in \{-1, 1\}$. Note that f is independent of the joint distribution of effective fields $W_{\sigma\tau}(u, v)$, so that it suffices to derive self-consistent equations for the distributions $W_\sigma(h)$ and $W_\tau(h)$. These are obtained by plugging eqs. (24-26) in eqs. (17-18) and taking the limit $n \rightarrow 0$

$$W_\sigma(h) = \sum_{k_\sigma, k_I=0}^{\infty} p_\sigma(k_\sigma) p_I(k_I) \int \left(\prod_{n=1}^{k_\sigma} dh_n W_\sigma(h_n) \right) \left(\prod_{m=1}^{k_I} dh_m W_\tau(h_m) \right) \times \delta \left[h - \mathcal{F}_\beta(h_1, \dots, h_{k_\sigma} | J_\sigma) - \mathcal{F}_\beta(h_1, \dots, h_{k_I} | U) \right], \quad (28)$$

$$W_\tau(h) = \sum_{k_\tau, k_I=0}^{\infty} p_\tau(k_\tau) p_I(k_I) \int \left(\prod_{n=1}^{k_\tau} dh_n W_\tau(h_n) \right) \left(\prod_{m=1}^{k_I} dh_m W_\sigma(h_m) \right) \times \delta \left[h - \mathcal{F}_\beta(h_1, \dots, h_{k_\tau} | J_\tau) - \mathcal{F}_\beta(h_1, \dots, h_{k_I} | U) \right], \quad (29)$$

where the degree distributions $p_\sigma(k)$, $p_\tau(k)$ and $p_I(k)$ are defined in eqs. (5-6), while the function \mathcal{F}_β reads

$$\mathcal{F}_\beta(h_1, \dots, h_K | J) = \frac{1}{\beta} \sum_{i=1}^K \operatorname{atanh} \left(\tanh(\beta h_i) \tanh(\beta J) \right). \quad (30)$$

The magnetizations of each network are given by

$$m_\sigma = \frac{1}{N} \sum_{i=1}^N \langle \sigma_i \rangle \quad m_\tau = \frac{1}{N} \sum_{i=1}^N \langle \tau_i \rangle. \quad (31)$$

In the present formalism, the magnetizations are obtained from the effective field distributions [31]:

$$m_\sigma = \int dh W_\sigma(h) \tanh(\beta h),$$

$$m_\tau = \int dh W_\tau(h) \tanh(\beta h).$$

Thus, once $W_\sigma(h)$ and $W_\tau(h)$ are determined from the solutions of eqs. (28) and (29), we can calculate the magnetizations of each network, obtain the phase diagrams, and probe the stability of the solutions through the free-energy.

4. Phase diagrams and metastability

For a general combination of model parameters, eqs. (28) and (29) cannot be analytically solved and one needs to employ a numerical approach. In this section we solve numerically eqs. (28) and (29) through the population dynamics method [32, 33], from which the phase diagrams and the free-energy follow. In this numerical approach, the distributions $W_\sigma(h)$ and $W_\tau(h)$ are parametrized, respectively, by large sets of stochastic variables $\{h_i^{(\sigma)}\}_{i=1, \dots, \mathcal{N}}$ and $\{h_i^{(\tau)}\}_{i=1, \dots, \mathcal{N}}$, with \mathcal{N} denoting the population size. By choosing initial distributions $W_\sigma^{(0)}(h)$ and $W_\tau^{(0)}(h)$ for each network, the variables $\{h_i^{(\sigma)}\}_{i=1, \dots, \mathcal{N}}$ and $\{h_i^{(\tau)}\}_{i=1, \dots, \mathcal{N}}$ are consistently updated according to the arguments

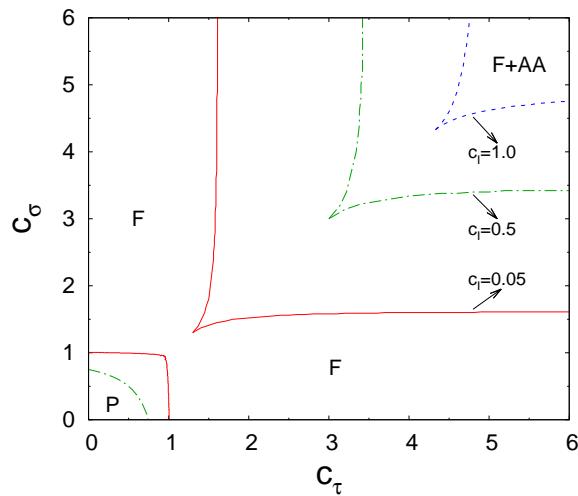


Figure 1. Phase diagram in the plane (c_σ, c_τ) for temperature $T = 0.001$, a value $U = 0.1$ for the coupling strength between the networks, and different values of the average connectivity c_I between the networks. The model displays a ferromagnetic solution (F), an anti-aligned (AA) solution, and a paramagnetic (P) state. The ferromagnetic and the anti-aligned solutions coexist in the region marked with F+AA, where the AA solution is always metastable. These results are obtained through the numerical solution of eqs. (28) and (29) using the population dynamics method with $\mathcal{N} = 5 \times 10^5$ and initial distributions $W_\sigma^{(0)}(h) = \delta(h - 1)$ and $W_\tau^{(0)}(h) = \delta(h + 1)$ (see the main text).

of the Dirac delta functions appearing in eqs. (28) and (29), until the empirical distribution obtained from each population of fields reaches its final, stationary form. Averages involving $W_\sigma(h)$ and $W_\tau(h)$ are evaluated by computing sample averages using, respectively, the collection of random variables $\{h_i^{(\sigma)}\}_{i=1, \dots, \mathcal{N}}$ and $\{h_i^{(\tau)}\}_{i=1, \dots, \mathcal{N}}$. We refer to [34] for further details regarding this numerical method.

From the numerical solutions of eqs. (28) and (29), we have calculated the magnetizations m_σ and m_τ of each network for different values of the model parameters. Three different solutions have been found: a paramagnetic state (P), with $m_\sigma = m_\tau = 0$; a ferromagnetic solution (F), where $m_\sigma m_\tau > 0$; and an anti-aligned state (AA), with $m_\sigma m_\tau < 0$.

In order to discuss the phase diagrams and the stability of these macroscopic states, we set $J_\sigma = J_\tau = 1$ throughout this section. Figure 1 shows typical phase diagrams in the (c_σ, c_τ) -plane for low temperatures and different values of c_I . The networks are weakly coupled with strength $U = 0.1$. For $J_\sigma = J_\tau$, the Hamiltonian is invariant with respect to the interchange of the adjacency matrix elements $c_{ij}^\sigma \leftrightarrow c_{ij}^\tau \forall i, j$, which implies on the symmetry of the above phase diagram around the straight line $c_\sigma = c_\tau$. In the region F+AA of figure 1, the ferromagnetic solution coexists with the (metastable) anti-aligned state [21, 23], namely, both types of order are obtained from the numerical solution of eqs. (28) and (29), depending on the initial distributions $W_\sigma^{(0)}(h)$ and $W_\tau^{(0)}(h)$ in the population dynamics method. As shown in figure 1, the anti-aligned solution is more

robust or more abundant in the phase diagram for strong modularity, i.e., when c_I is much smaller than the mean connectivities within each network. In the paramagnetic phase, the effective field distributions are given by $W_\sigma(h) = W_\tau(h) = \delta(h)$. The distributions $W_\sigma(h)$ and $W_\tau(h)$ have a small average close to the boundary between the P and F phases, which allows to expand the right hand side of eqs. (28) and (29) and derive the equation for the boundary between these states

$$c_I^2 \tanh^2(\beta U) = [1 - c_\sigma \tanh(\beta J_\sigma)] [1 - c_\tau \tanh(\beta J_\tau)] . \quad (32)$$

From the above equation, one concludes that the system exhibits a paramagnetic phase for $T = 0$, located in a region of the phase diagram where all average connectivities must be smaller than one. This is consistent with figure 1, in which the P phase is absent for $c_I = 1$. The reason for the existence of this zero-temperature P phase is utterly topological, since for low connectivities the system is fragmented in a large number of finite non-interacting clusters [5].

Figure 2 complements the phase diagram of figure 1 by showing results for the critical coupling strength U_c above which the anti-aligned solution is absent, considering different values of T and c_I . The parameter $c \equiv c_\tau = c_\sigma$ is the average connectivity within each network. As can be noted, the increase of T or c_I has a detrimental effect on the existence of anti-aligned states. Below we study in more detail the effect of thermal fluctuations in the stability of such states. The curves in figure 2 converge to $c = c_{\text{perc}}(T)$ as $U \rightarrow 0$, where $c_{\text{perc}}(T)$ is the critical average connectivity above which a single random graph lies in a ferromagnetic state. We have that $c_{\text{perc}}(T) \simeq 1$ for the smallest temperature displayed in figure 2, consistent with standard results for the percolation transition in random graphs [5].

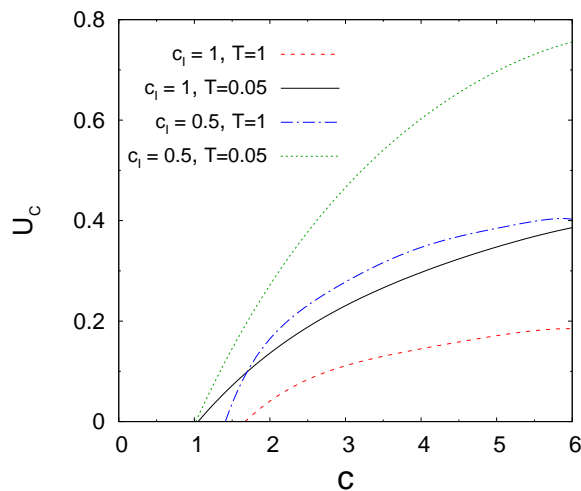


Figure 2. Critical coupling strength U_c below which we find an anti-aligned solution from eqs. (28) and (29). The results are shown as a function of the average connectivity $c \equiv c_\sigma = c_\tau$ within each network, for different combinations of temperature T and the average connectivity c_I between the networks. We have rescaled all coupling constants (see eq. (1)) by the common factor $c_{\text{eff}} = \frac{1}{3}(c_\sigma + c_\tau + c_I)$. These results are obtained through the numerical solution of eqs. (28) and (29) using the population dynamics method with $\mathcal{N} = 5 \times 10^5$ and initial distributions $W_\sigma^{(0)}(h) = \delta(h - 1)$ and $W_\tau^{(0)}(h) = \delta(h + 1)$ (see the main text).

In figure 3(a) we show the absolute value of the magnetization of a single network along the straight line $c_\sigma = c_\tau$ of the phase diagram, considering initial distributions $W_\sigma^{(0)}(h) = \delta(h - 1)$ and $W_\tau^{(0)}(h) = \delta(h + 1)$ that yield $m_\sigma > 0$ and $m_\tau < 0$ in the region F+AA. As clearly shown, the transition between the paramagnetic and the F state is continuous, while the magnetization changes discontinuously along the boundary between the F region and the F+AA region. In this case, such discontinuity is not a signature of a first-order phase transition, but it simply reflects the sudden emergence of the metastable anti-aligned solution. The equilibrium magnetization, characterized by a continuous branch, is not shown when $c_\sigma = c_\tau$ lies in the F+AA region, since eqs. (28) and (29) have been solved with initial distributions favouring the anti-aligned solution. The stability of the different solutions is characterized in figure 3(b), where we present the free-energy f of each possible solution of eqs. (28) and (29) as a function of $c_\sigma = c_\tau$, for a single value of c_I ‡. The main outcome is that the anti-aligned solution is always metastable, while the ferromagnetic solution is the stable macroscopic state, since it corresponds to the global minimum of the free-energy. We have checked many different combinations of model parameters and we did not find any qualitative changes in these stability properties. All results discussed in this section are also applied to the case where the couplings between the networks are anti-ferromagnetic. The difference is that, for $U < 0$, the ferromagnetic solution is metastable, while the anti-aligned solution is the stable macroscopic state. Apart from that, the phase diagrams remain unchanged, i.e., the phase boundaries for $U < 0$ are the same as those for $U > 0$.

‡ The free-energy of the paramagnetic solution is displayed only for model parameters within the region P, where the paramagnetic state is the only possible solution of eqs. (28) and (29). In regions F and F+AA, figure 3(b) exhibits only the free-energy of the nontrivial states.

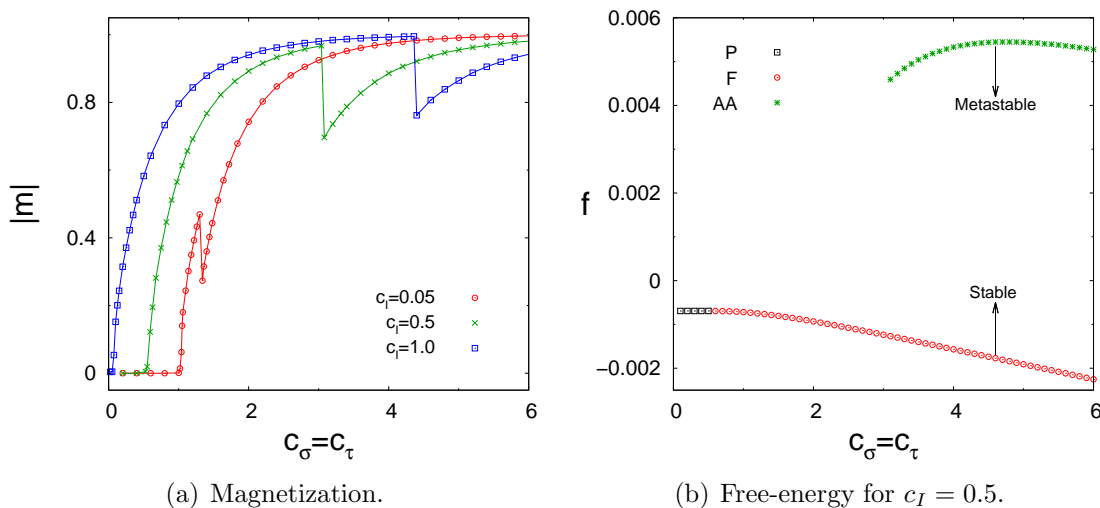


Figure 3. Absolute value of the magnetization $|m|$ of a single network and free-energy per spin f as functions of $c_\sigma = c_\tau$ for temperature $T = 0.001$ and ferromagnetic coupling $U = 0.1$. The values of the average connectivity c_I between the networks are indicated on the graphs. The magnetizations of each network have the same absolute value for $c_\sigma = c_\tau$. The three different solutions of the phase diagram and the corresponding free-energies are shown here. These results are obtained through the population dynamics method with $\mathcal{N} = 10^6$ and initial distributions $W_\sigma^{(0)}(h) = \delta(h-1)$ and $W_\tau^{(0)}(h) = \delta(h+1)$ (see the main text).

5. Numerical simulations

In this section we compare our theoretical results with Monte-Carlo (MC) simulations using standard Metropolis dynamics of finite size systems with different system sizes. We also compute the typical time the system needs to escape from the metastable states. This is a way to go beyond the theoretical results and quantify the lifetime of the metastable states and have a better idea of their role on the relaxation of the system to equilibrium.

The theoretical results indicating a second order phase transition from a paramagnetic to a ferromagnetic phase, where metastable anti-aligned states appear for certain model parameters, are verified in the MC simulations. We have measured the magnetizations of each network in equilibrium or in metastable configurations, following a quasi-static heating protocol of the system prepared initially at zero temperature in a purely anti-aligned metastable state, where the spins in different networks have opposite directions. Simulations were done for $J_\sigma = J_\tau = U = 1/c_{\text{eff}}$, with $c_{\text{eff}} = \frac{1}{3}(c_\sigma + c_\tau + c_I)$, and two cases of average connectivities $c_\sigma = c_\tau = 10$ and $c_I = 1.0$, and $c_\sigma = c_\tau = 4$ and $c_I = 0.5$. Simulated system sizes range from $N = 400$ up to $N = 25600$, where N stands for the number of nodes in each graph. Equilibration times in each temperature are of order 10^5 MC steps, and averages are taken from 100 different realizations of the random graphs, each realization contributing with 100 samples for each temperature.

Figure 4 shows the comparison between MC simulations and our theoretical results

for the magnetization of each network as a function of the temperature. As can be noticed, finite size effects in MC simulations become remarkable as T increases towards the instability temperature, above which the anti-aligned metastable state disappears. This is a purely dynamical effect in the heating protocol, due to the available thermal energy and finite energy barrier between the metastable state and the true thermodynamical equilibrium state. In spite of that, the overall agreement between our theory and MC simulations is excellent, with the simulation data consistently approaching the theoretical curves for increasing N .

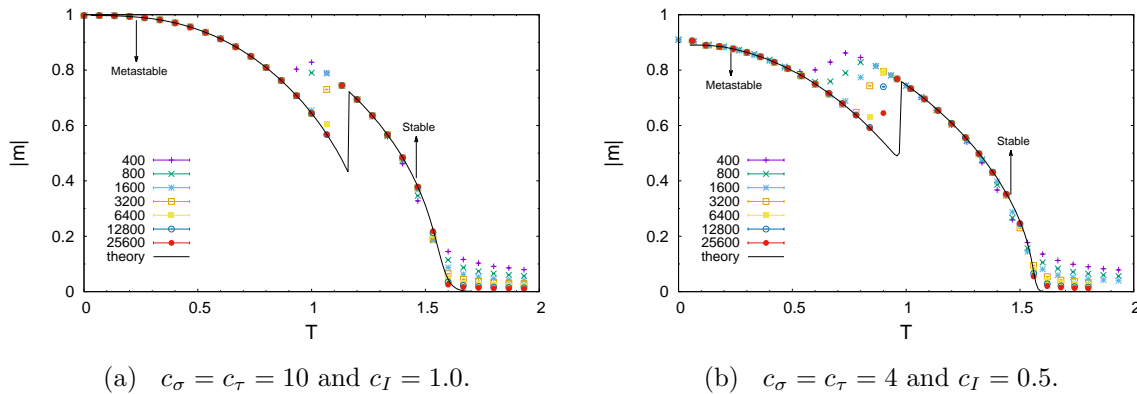


Figure 4. Results for the magnetization $|m|$ of each network as a function of the temperature T for coupling strengths $J_\sigma = J_\tau = U = 1/c_{\text{eff}}$, with $c_{\text{eff}} = \frac{1}{3}(c_\sigma + c_\tau + c_I)$. The magnetization of each graph has the same absolute value for $c_\sigma = c_\tau$. Each panel compares the theoretical results, derived from the solutions of eqs. (28) and (29), with Monte-Carlo simulations following a heating protocol started at $T = 0$ in the metastable anti-aligned state, for different systems sizes N , whose values are shown on each graph. Equations (28) and (29) are solved numerically using the population dynamics method with $\mathcal{N} = 10^6$ and initial distributions $W_\sigma^{(0)}(h) = \delta(h - 1)$ and $W_\tau^{(0)}(h) = \delta(h + 1)$ (see the main text).

We have also computed the average or typical time τ for the system to escape from a metastable anti-aligned state. By preparing the system in an initial configuration corresponding to the zero temperature anti-aligned solution, with $m_\sigma = 1$ and $m_\tau = -1$, the parameter τ counts the average number of MC steps that the system needs to reach a configuration in which one of the magnetizations changes sign. Averages are taken from 100 to 2000 different realizations of the random graphs. Figure 5(a) exhibits τ as a function of T for the same combination of model parameters as in figure 4(a). The simplest temperature dependence of these results is well described, especially in the region where τ increases abruptly, by the Vogel-Fulcher law $\tau(T) = A \exp\left(\frac{E}{T - T_0}\right)$, where the parameters A , E and T_0 depend on N .

Figure 5(a) strongly indicates that, in the limit $N \rightarrow \infty$, the typical time τ diverges as $T \rightarrow T_{\text{ins}}^+$, where T_{ins} is the temperature above which metastable states are absent in the thermodynamic limit. Such divergent behaviour is confirmed in figure 5(b), where we show the exponential divergence of $\tau = B \exp(bN)$ as a function of the system size

for $T = 1.105 < T_{\text{ins}}$, with resulting fitting parameters $B = 37(4)$ and $b = 0.00044(1)$. This typically characterizes a thermally activated process of crossing free-energy barriers [35], which is consistent with the mean-field character of our model, or with the fact that the free-energy barriers separating different macroscopic states are proportional to N . Thus, as long as $T < T_{\text{ins}}$ and $N \rightarrow \infty$, the system becomes trapped in the metastable states, once it is prepared in a configuration close to them.

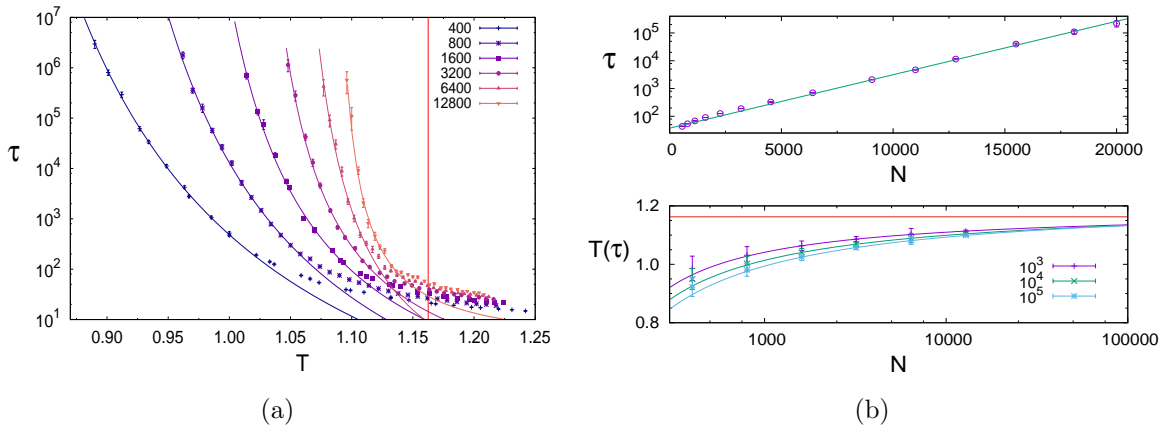


Figure 5. (a) Results obtained from Monte-Carlo simulations for the average time τ that it takes for the system to escape from a metastable anti-aligned state (see the main text) as a function of temperature. The values of the average connectivities are $c_\sigma = c_\tau = 10$ and $c_I = 1$, while the coupling strengths are given by $J_\sigma = J_\tau = U = 1/c_{\text{eff}}$, with $c_{\text{eff}} = \frac{1}{3}(c_\sigma + c_\tau + c_I)$. The different system sizes N are indicated on the graph. Lines are fits to $\tau(T) = A \exp(E/(T - T_0))$, and the vertical line corresponds to the theoretical result for the instability temperature $T_{\text{ins}} = 1.163$. (b) The upper figure displays the behaviour of τ as a function of N for $T = 1.105$, where the line corresponds to an exponential fit (see the main text). The lower figure shows the system size dependence of the temperatures for which each fit in figure (a) gives a fixed average time τ . The curves are fits of the form $T(\tau) = T_0 + a/\ln(bN)$, and the horizontal line is the instability temperature $T_{\text{ins}} = 1.163$ in the limit $N \rightarrow \infty$.

The instability temperature can be extracted from the simulation data by inverting the fits in figure 5(a) to obtain $T(\tau)$, the temperatures at which, for a given size, the system takes on average τ MC steps to cross the free-energy barrier. Data for $\tau = 10^3$, 10^4 and 10^5 are shown in figure 5(b). The extrapolation of T_0 for $N \rightarrow \infty$ can be performed by fitting the curves with $T_0 + a/\log(bN)$. The resulting values for T_0 are 1.19(1), 1.20(1) and 1.22(1), respectively, for $\tau = 10^3$, 10^4 and 10^5 , which agrees well with our theoretical result $T_{\text{ins}} = 1.163$, strictly valid for $N \rightarrow \infty$.

6. Final remarks

In this work we have studied the phase diagram and the existence of metastable states in a simple model of coupled networks. The model is composed of two coupled Erdős-Rényi random graphs with an Ising state variable or spin lying at each node. Each spin

in a given graph has a finite number of ferromagnetic couplings within its own graph and ferromagnetic interactions with a finite subset of spins located on the other graph. The simplicity of this model has enabled us to exactly compute the magnetization of each network and the free-energy of the system in the thermodynamic limit, using the replica method of disordered systems. The main outcome of our work is the full characterization of the phase diagram and of the stability properties of the different macroscopic states. As we clearly illustrate through the computation of the free-energy, the ferromagnetic solution is the thermodynamic state, while the anti-aligned solution (magnetizations with opposite signs) is always metastable. The metastable solution appears through a discontinuous transition as a function of the model parameters, provided the average connectivity within each network is large enough and the temperature is sufficiently low.

We have estimated, through Monte-Carlo simulations, the average time τ the system needs to escape from a metastable configuration. Our results for $\tau(T)$ are well-described by the Vogel-Fulcher law, which tells us that there is a critical temperature below which τ diverges in the thermodynamic limit $N \rightarrow \infty$. Such ergodicity breaking stems from the mean-field character of our model, in which the free-energy barrier between the metastable and the stable macroscopic state diverges for $N \rightarrow \infty$. Our main theoretical results have been compared with Monte-Carlo simulations, showing a very good agreement.

We have also shown that the phase diagram, as defined in the space of the connectivities of each network, exhibits a low-temperature paramagnetic phase for very small average connectivities. This is explained by the fact that, in this sector of the phase diagram, the random graphs are fragmented in a large number of disconnected finite clusters that are unable to communicate. Finally, we point out that the present work paves the way to pursue a detailed study of the cooperative behaviour arising in coupled networks with different architectures [36, 37], such as modular and core-periphery structures. Work along these lines is underway.

Acknowledgments

The authors thank Massimo Ostilli for a critical reading of the manuscript. L.N. thanks the hospitality of Universidade Federal de Santa Maria, Brazil. M.B. acknowledges a fellowship from CAPES. F.L.M. thanks London Mathematical Laboratory and CNPq (Edital Universal 406116/2016-4) for financial support.

References

- [1] A. Barrat, M. Barthlemy, and A. Vespignani, *Dynamical Processes on Complex Networks*. New York, NY, USA: Cambridge University Press, 1st ed., 2008.
- [2] Y. Deng, Y.-H. Jiang, Y. Yang, Z. He, F. Luo, and J. Zhou, “Molecular ecological network analyses,” *BMC Bioinformatics*, vol. 13, p. 113, May 2012.
- [3] Z. D. Kurtz, C. L. Mller, E. R. Miraldi, D. R. Littman, M. J. Blaser, and R. A. Bonneau, “Sparse

- and compositionally robust inference of microbial ecological networks,” *PLOS Computational Biology*, vol. 11, pp. 1–25, 05 2015.
- [4] T. Squartini, I. V. Lelyveld, and D. Garlaschelli, “Early-warning signals of topological collapse in interbank networks,” *Scientific Reports*, vol. 3, p. 3357, 2013.
 - [5] S. N. Dorogovtsev, A. V. Goltsev, and J. F. F. Mendes, “Critical phenomena in complex networks,” *Rev. Mod. Phys.*, vol. 80, pp. 1275–1335, Oct 2008.
 - [6] T. Nishikawa, A. E. Motter, Y.-C. Lai, and F. C. Hoppensteadt, “Heterogeneity in oscillator networks: Are smaller worlds easier to synchronize?,” *Phys. Rev. Lett.*, vol. 91, p. 014101, Jul 2003.
 - [7] J. Gómez-Gardeñes, Y. Moreno, and A. Arenas, “Paths to synchronization on complex networks,” *Phys. Rev. Lett.*, vol. 98, p. 034101, Jan 2007.
 - [8] C. Castellano, S. Fortunato, and V. Loreto, “Statistical physics of social dynamics,” *Rev. Mod. Phys.*, vol. 81, pp. 591–646, May 2009.
 - [9] R. Baxter, *Exactly Solved Models in Statistical Mechanics*. Dover books on physics, Dover Publications, 2007.
 - [10] M. Leone, A. Vázquez, A. Vespignani, and R. Zecchina, “Ferromagnetic ordering in graphs with arbitrary degree distribution,” *The European Physical Journal B - Condensed Matter and Complex Systems*, vol. 28, pp. 191–197, Jul 2002.
 - [11] R. Lambiotte, M. Ausloos, and J. A. Holyst, “Majority model on a network with communities,” *Phys. Rev. E*, vol. 75, p. 030101, Mar 2007.
 - [12] J.-P. Bouchaud, “Crises and collective socio-economic phenomena: Simple models and challenges,” *Journal of Statistical Physics*, vol. 151, pp. 567–606, May 2013.
 - [13] J. Gao, S. V. Buldyrev, H. E. Stanley, and S. Havlin, “Networks formed from interdependent networks,” *Nature Physics*, vol. 8, pp. 40–48, 2012.
 - [14] M. Kivel, A. Arenas, M. Barthélemy, J. P. Gleeson, Y. Moreno, and M. A. Porter, “Multilayer networks,” *Journal of Complex Networks*, vol. 2, no. 3, pp. 203–271, 2014.
 - [15] J. Gao, D. Li, and S. Havlin, “From a single network to a network of networks,” *National Science Review*, vol. 1, no. 3, pp. 346–356, 2014.
 - [16] V. Rosato, L. Issacharoff, F. Tiriticco, S. Meloni, S. Porcellinis, and R. Setola, “Modelling interdependent infrastructures using interacting dynamical models,” *Int. J. Crit. Infrastruct.*, vol. 4, pp. 63–79, 2008.
 - [17] S. V. Buldyrev, R. Parshani, G. Paul, H. E. Stanley, and S. Havlin, “Catastrophic cascade of failures in interdependent networks,” *Nature*, vol. 464, pp. 1025–1028, 2010.
 - [18] M. Girvan and M. E. J. Newman, “Community structure in social and biological networks,” *Proceedings of the National Academy of Sciences*, vol. 99, no. 12, pp. 7821–7826, 2002.
 - [19] J.-P. Onnela, J. Saramäki, J. Hyvönen, G. Szabó, D. Lazer, K. Kaski, J. Kertész, and A.-L. Barabási, “Structure and tie strengths in mobile communication networks,” *Proceedings of the National Academy of Sciences*, vol. 104, no. 18, pp. 7332–7336, 2007.
 - [20] G. Palla, I. Derényi, I. Farkas, and T. Vicsek, “Uncovering the overlapping community structure of complex networks in nature and society,” *Nature*, vol. 435, pp. 814–818, 2005.
 - [21] K. Suchecki and J. A. Holyst, “Ising model on two connected barabasi-albert networks,” *Phys. Rev. E*, vol. 74, p. 011122, Jul 2006.
 - [22] S. Dasgupta, R. K. Pan, and S. Sinha, “Phase of ising spins on modular networks analogous to social polarization,” *Phys. Rev. E*, vol. 80, p. 025101, Aug 2009.
 - [23] K. Suchecki and J. A. Holyst, “Bistable-monostable transition in the ising model on two connected complex networks,” *Phys. Rev. E*, vol. 80, p. 031110, Sep 2009.
 - [24] M. Ostilli and J. F. F. Mendes, “Communication and correlation among communities,” *Phys. Rev. E*, vol. 80, p. 011142, Jul 2009.
 - [25] E. Agliari, R. Burioni, and P. Sgrignoli, “A two-populations ising model on diluted random graphs,” *Journal of Statistical Mechanics: Theory and Experiment*, vol. 2010, no. 07, p. P07021, 2010.
 - [26] H. Chen and Z. Hou, “Optimal modularity for nucleation in a network-organized ising model,”

- Phys. Rev. E*, vol. 83, p. 046124, Apr 2011.
- [27] H. Feng, C. Han-Shuang, and S. Chuan-Sheng, “Phase transitions of majority-vote model on modular networks,” *Chinese Physics Letters*, vol. 32, no. 11, p. 118902, 2015.
- [28] B. Bollobás, *Random Graphs*. Cambridge University Press, second ed., 2001. Cambridge Books Online.
- [29] M. Mezard, G. Parisi, and M. Virasoro, *Spin Glass Theory and Beyond*. Lecture Notes in Physics Series, World Scientific, 1987.
- [30] M. Mézard and G. Parisi, “Mean-field theory of randomly frustrated systems with finite connectivity,” *EPL (Europhysics Letters)*, vol. 3, no. 10, p. 1067, 1987.
- [31] R. Monasson, “Optimization problems and replica symmetry breaking in finite connectivity spin glasses,” *Journal of Physics A: Mathematical and General*, vol. 31, no. 2, p. 513, 1998.
- [32] M. Mézard and G. Parisi, “The bethe lattice spin glass revisited,” *The European Physical Journal B - Condensed Matter and Complex Systems*, vol. 20, no. 2, pp. 217–233, 2001.
- [33] M. Mézard and G. Parisi, “The cavity method at zero temperature,” *Journal of Statistical Physics*, vol. 111, no. 1, pp. 1–34, 2003.
- [34] M. Mezard and A. Montanari, *Information, Physics, and Computation*. New York, NY, USA: Oxford University Press, Inc., 2009.
- [35] K. Brendel, G. T. Barkema, and H. van Beijeren, “Magnetization reversal times in the two-dimensional ising model,” *Phys. Rev. E*, vol. 67, p. 026119, Feb 2003.
- [36] E. Estrada, “Topological structural classes of complex networks,” *Phys. Rev. E*, vol. 75, p. 016103, Jan 2007.
- [37] P. Csermely, A. London, L.-Y. Wu, and B. Uzzi, “Structure and dynamics of core/periphery networks,” *Journal of Complex Networks*, vol. 1, no. 2, pp. 93–123, 2013.